



Article

Cascading Effects of Nanoparticle Coatings: Surface Functionalization Dictates the Assemblage of Complexed Proteins and Subsequent Interaction with Model Cell Membranes

Eric S Melby, Samuel E. Lohse, Ji Eun Park, Ariane M. Vartanian, Rebecca A Putans, Hannah B. Abbott, Robert J Hamers, Catherine J. Murphy, and Joel A. Pedersen

ACS Nano, Just Accepted Manuscript • Publication Date (Web): 08 May 2017

Downloaded from http://pubs.acs.org on May 15, 2017

Just Accepted

"Just Accepted" manuscripts have been peer-reviewed and accepted for publication. They are posted online prior to technical editing, formatting for publication and author proofing. The American Chemical Society provides "Just Accepted" as a free service to the research community to expedite the dissemination of scientific material as soon as possible after acceptance. "Just Accepted" manuscripts appear in full in PDF format accompanied by an HTML abstract. "Just Accepted" manuscripts have been fully peer reviewed, but should not be considered the official version of record. They are accessible to all readers and citable by the Digital Object Identifier (DOI®). "Just Accepted" is an optional service offered to authors. Therefore, the "Just Accepted" Web site may not include all articles that will be published in the journal. After a manuscript is technically edited and formatted, it will be removed from the "Just Accepted" Web site and published as an ASAP article. Note that technical editing may introduce minor changes to the manuscript text and/or graphics which could affect content, and all legal disclaimers and ethical guidelines that apply to the journal pertain. ACS cannot be held responsible for errors or consequences arising from the use of information contained in these "Just Accepted" manuscripts.



Cascading Effects of Nanoparticle Coatings: Surface Functionalization Dictates the Assemblage of Complexed Proteins and Subsequent Interaction with Model Cell Membranes

Eric S. Melby, ^{1,†,‡} Samuel E. Lohse, ^{2,†,§} Ji Eun Park, ^{2,†} Ariane M. Vartanian, ^{2,¶}Rebecca A. Putans, ^{3,#} Hannah B. Abbott, ¹ Robert J. Hamers, ³ Catherine J. Murphy, ^{2,*} Joel A. Pedersen, ^{1,3,*}

* Corresponding Authors:

Joel A. Pedersen; University of Wisconsin, 1525 Observatory Drive, Madison, WI, 53706; 608-263-4971; joelpedersen@wisc.edu

<u>Catherine J. Murphy</u>; University of Illinois, A512 CLSL, Box 59-6, 600 South Mathews Avenue, Urbana, IL 61801; (217)333-7680; <u>murphycj@illinois.edu</u>

KEYWORDS: gold nanoparticle, protein corona, surface chemistry, supported lipid bilayer

¹ University of Wisconsin-Madison, Environmental Chemistry and Technology Program, 1525 Observatory Dr., Madison, WI, 53706

² University of Illinois at Urbana-Champaign, Department of Chemistry, 600 S. Mathews Ave., Urbana, IL, 61801

³ University of Wisconsin-Madison, Department of Chemistry, 1101 University Ave., Madison, WI, 53706

[†] These authors contributed equally to this work.

[‡] Present address: Pacific Northwest National Laboratory, Richland, WA 99352

[§] Present address: Colorado Mesa University, Department of Chemistry, 1100 North Ave, Grand Junction, CO, 81501

Present address: Northwestern University, Department of Chemistry, Evanston, IL 60208

[¶] Present address: Nature Communications, 1 New York Plaza, 1 FDR Dr., New York, NY 10004

[#] Present address: Dow Chemical Company, 1712 S. Saginaw Rd, Midland, MI 48674

ABSTRACT: Interactions of functionalized nanomaterials with biological membranes are expected to be governed by not only nanoparticle physiochemical properties, but also coatings or "coronas" of biomacromolecules acquired after emersion in biological fluids. Here, we prepared a library of 4-5 nm gold nanoparticles (AuNPs) coated with either ω-functionalized thiols or polyelectrolyte wrappings to examine the influence of surface functional groups on the assemblage of proteins complexing the nanoparticles and its subsequent impact on attachment to model biological membranes. We find that the initial nanoparticle surface coating has a cascading effect on interactions with model cell membranes by determining the assemblage of complexing proteins which in turn influences subsequent interaction with model biological membranes. Each type of functionalized AuNP investigated formed complexes with a unique ensemble of serum proteins that depended on the initial surface coating of the nanoparticles. Formation of protein-nanoparticle complexes altered the electrokinetic, hydrodynamic, and plasmonic properties of the AuNPs. Complexation of the nanoparticles with proteins reduced the attachment of cationic AuNPs and promoted attachment of anionic AuNPs to supported lipid bilayers; this trend is observed with both lipid bilayers comprised of 100% zwitterionic phospholipids and those incorporating anionic phosphatidylinositol. Complexation with serum proteins led to attachment of otherwise non-interacting oligo(ethylene glycol)-functionalized AuNPs to bilayers containing phosphatidylinositol. These results demonstrate the importance of considering both facets of the nano-bio interface: functional groups displayed on the nanoparticle surface and proteins complexing the nanoparticles influence interaction with biological membranes molecular themselves. as does the makeup of the membranes

Upon introduction into biological fluids (e.g., blood, lymph, cytoplasm, respiratory tract fluid, cell culture media), nanoparticles (NPs) acquire coatings of biomolecules, of which

proteins have received the most attention, commonly referred to as "coronas". ¹⁻⁶ Acquisition of a protein corona increases the effective diameter of nanoparticles, alters their surface properties, and can affect nanoparticle aggregation state. ^{1-5,7-10} The surface properties of nanoparticles in biological milieux thus diverge from those that the nanoparticle was engineered to possess, impacting their interactions with cellular membranes and receptors. ^{1-5,7-10} Nanoparticles surrounded by a biomolecular corona possess a "biological identity" that differs from their initial "synthetic identity". ¹¹ The amount, composition, and orientation of biomolecules present on the surface of nanoparticles strongly influence their adsorption, distribution, and elimination in biological systems and dominate their interactions with cellular membranes and receptors. ^{1-5,7-10} Despite the importance of the biomolecular corona in governing nanoparticle interactions at biological interfaces, the influence of protein corona formation on nanoparticle behavior at biological membranes has only recently begun to receive detailed study. ^{5,14-16}

Protein association with nanoparticles is commonly discussed in terms of a tightly adsorbed layer ("hard" corona) surrounded by a more loosely bound layer ("soft" corona).^{3,13} This distinction is widely accepted and is useful to differentiate proteins with long residence times on the particle surface from those that are susceptible to more rapid exchange with the surrounding solution. The applicability of the protein corona concept has been questioned for small nanoparticles with diameters similar to the proteins associating with their surface.¹⁷ In this paper, we refer to nanoparticles with surface-associated proteins as protein-nanoparticle complexes.

To date, the majority of experimental studies on the interactions of nanoparticles with biological systems have focused on those with core diameters between 20-400 nm. ^{1-5,7-10,17} Interactions of nanoparticles with core diameters less than 5 nm, on the same length scale of

many proteins, with biological systems have received less attention. ^{18,19} Understanding biological interactions of these small nanoparticles is crucial because they (i) can passively penetrate, and in some cases disrupt, cellular membranes; ^{20–23} (ii) often exhibit higher toxicity *in vitro* and in whole organism models relative to larger nanoparticles of the same core material; ²⁴ (iii) are similar in size to many common serum proteins (*e.g.*, the longest dimension of human serum albumin is ~7.5 nm); ^{14,25} and (iv) may function more effectively as nanotherapeutics than larger nanoparticles. ⁴ At present, the influence of the surface functional groups of small nanoparticles on the selection of complexing proteins has received little study and the subsequent interaction of such protein-nanoparticle complexes with biological membranes is poorly understood.

The objectives of this study were (1) to test the hypothesis that the surface charge and structure of functionalizing molecules on small nanoparticles control the identity of complexed proteins; and (2) to investigate the influence of complexed proteins on nanoparticle interaction with models of biological membranes. To accomplish these objectives, we prepared a library of ~4-5 nm AuNPs functionalized with ligands presenting negatively charged, neutral or positively charged moieties to solution or wrapped with negatively or positively charged polyelectrolytes (Figure 1). Gold nanoparticles were selected for study because their physicochemical properties (size, shape, and surface functional groups) can be precisely controlled. ²⁶⁻²⁸ The nanoparticle surface functionalizations chosen for these experiments were previously used in a number of studies to investigate the effects of surface functionalization of 4 nm AuNP on toxicity to model organisms (e.g., Daphnia magna, Shewanella oneidensis) as well as on interaction with supported lipid bilayer binding studies. ^{22,29-31} We exposed these nanoparticles to serum proteins, isolated protein-AuNP complexes using a procedure previously employed to operationally define

the hard corona of larger nanoparticles,³² and identified the proteins in complexes with nanoparticles by liquid chromatography-tandem mass spectrometry (LC-MS/MS). We used supported lipid bilayers composed of phospholipids bearing zwitterionic phosphatidylcholine (PC) headgroups or a mixture of PC and phosphatidylinositol (PI) phospholipids as simple models to examine the influence of complexed proteins on AuNP interaction with biological membranes.

RESULTS AND DISCUSSION

Physiochemical Properties of the Functionalized AuNPs. We synthesized a library of ~4-5 nm AuNPs functionalized with either ligands anchored to the AuNP surface *via* a thiol group or wrapped with polyelectrolytes (Figure 1). The ligand-functionalized AuNP displayed positively charged (mercaptopropylamine, MPNH₂), neutral (mercapto undecanethiolethyleneglycol hexamer, EG₀),³³ or negatively charged (mercaptopropionic acid, MPA) ω-functional groups to solution. Polyelectrolytes used to wrap AuNPs included positively charged (poly(allylamine hydrochloride), PAH) and negatively charged (polyacrylic acid, PAA). The effect of these ligands and coatings (specifically PAH and MPA) anchored to 4 nm AuNP on acute and chronic toxicity, as well as on transcriptional responses, has previously been tested in (and compared between) the planktonic microcrustacean *D. magna* and the Gram-negative bacterium *S. oneidensis*.²⁹ We therefore employed the nanoparticles shown in Figure 1 for the present studies to enable connection to multiple organism data sets. The 4 nm PAH- and MPA-AuNPs were also previously used as nanoparticle probes in studies on binding to model membranes, in the absence of serum proteins.^{22,30,31}

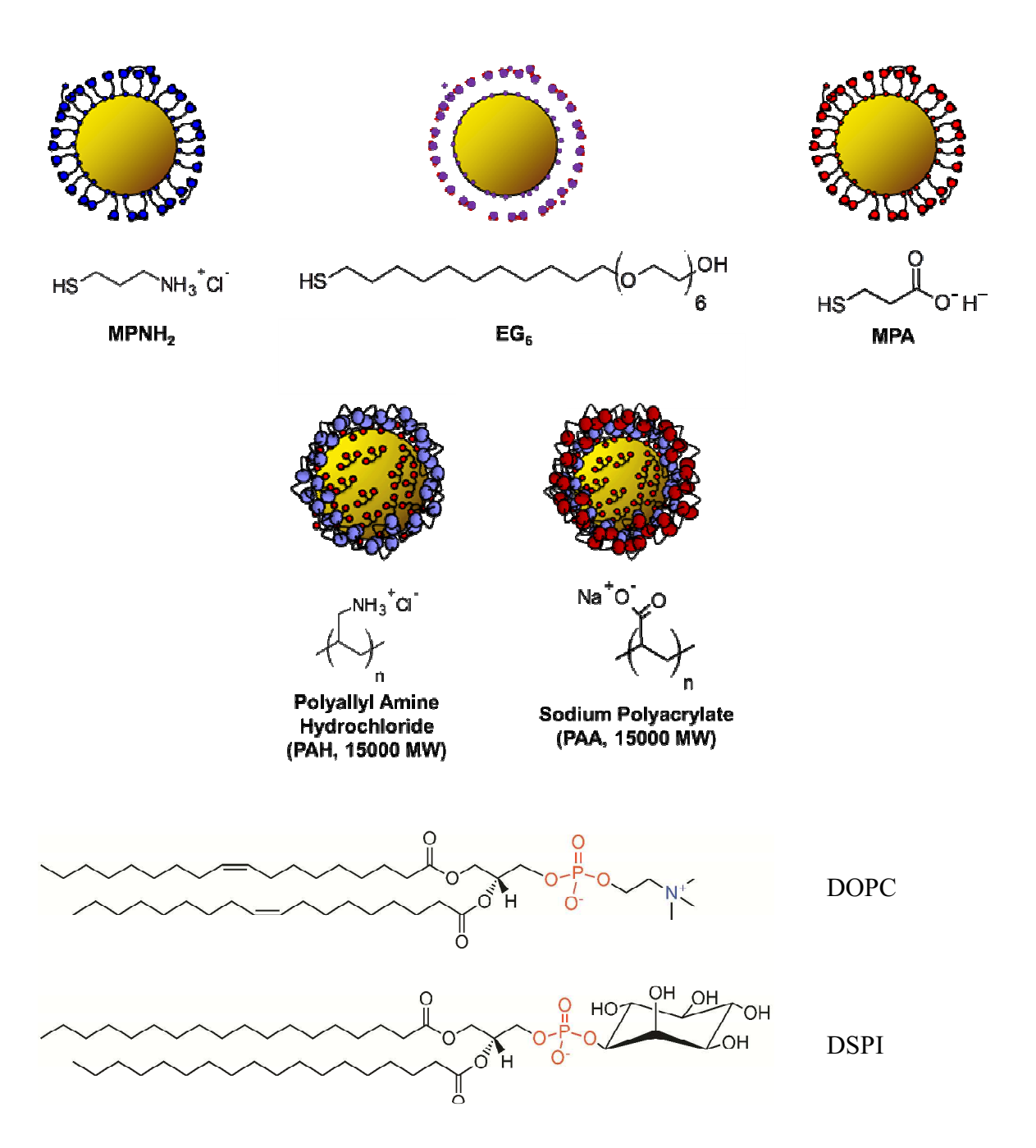
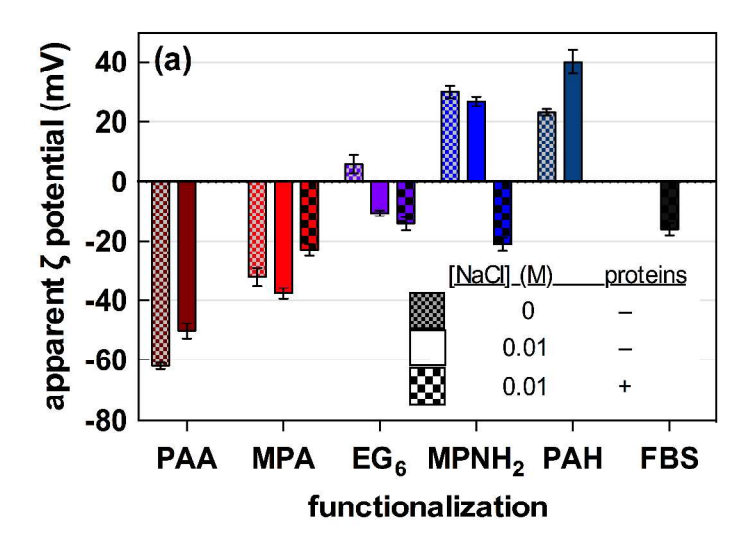


Figure 1. Functionalized AuNPs and phospholipids used in this study. Abbreviations: DOPC, 1,2-dioleoyl-sn-glycero-3-phosphocholine; DSPI, 1,2-distearoyl-sn-glycero-3-phosphoinositol; EG₆, mercapto undecanethiol-ethyleneglycol hexamer; MPA, mercaptoproionic acid; MPNH₂, mercaptopropylamine; PAA, polyacrylic acid; PAH, poly(allylamine HCl). DSPI is the most abundant lipid in bovine liver α-phosphatidylinositol.

We determined the size of the functionalized AuNPs by visible absorbance spectroscopy and transmission electron microscopy (TEM).³⁴ Suspensions of all AuNPs in ultrapure water

(≥18 M Ω ·cm resistivity) exhibited plasmon absorbance wavelength maxima (λ_{max}) at ~520 nm, consistent with the presence of 4-5 nm AuNPs (Table S1, Figure S1).³⁴ Analysis of TEM images confirmed that AuNP core diameters (d_{core}) were statistically equivalent, regardless of the subsequent surface functionalization employed (Figures S2 and S3): MPNH₂-AuNPs (4.4 ± 1.5 nm, n = 420), EG₆-AuNPs (4.1 ± 1.1 nm, n = 1295), MPA-AuNPs (4.2 ± 1.2 nm, n = 451), PAH-AuNPs ($d_{core} = 4.7 \pm 1.5 \text{ nm}, n = 381$), and PAA-AuNPs ($4.9 \pm 1.4 \text{ nm}, n = 530$). Dynamic light scattering measurements of the AuNPs dispersed in ultrapure water indicated that the number mean hydrodynamic diameters $(d_{h,n})$ were 5-10 nm for the thiol-functionalized AuNPs (Table S1), consistent with monodisperse suspensions. The hydrodynamic diameters of the PAH- and PAA-AuNPs were 17.9 ± 0.9 nm and 56.7 ± 1.3 nm, respectively. Considering that the mean core diameters of the polyelectrolyte-wrapped AuNPs (as determined by TEM) were 4-5 nm, the relatively large hydrodynamic diameters observed for the polyelectrolyte-wrapped AuNPs indicates the formation of aggregates during the polyelectrolyte wrapping process as well as the presence of regions of the polyelectrolyte chain that extend into solution. The visible absorbance spectra of these AuNPs indicate that their aggregation did not bring the gold cores into sufficient proximity to impact their plasmonic properties.^{35,36} The (apparent) ζ potentials of the AuNPs in ultrapure water were consistent with the expected surface charges imparted by their respective ligands, although the EG₆-functionalized particles had negative ζ potentials (Figure 2a). Charge screening caused by the transfer of the AuNPs from ultrapure water to a 0.01 M NaCl solution buffered to pH 7.4 with 0.01 M Tris resulted in a significant reduction in the magnitude of the apparent ζ potential for EG₆-, MPNH₂-, and PAH-AuNPs (p < 0.01; Figure 2a, Table S1). Changes in apparent ζ potential of the MPA- and PAA-AuNPs were not statistically significant. Transfer of the functionalized AuNPs from ultrapure water to 0.01 M NaCl resulted in increases

in the hydrodynamic diameters of MPA-, MPNH₂-, and PAH-AuNPs (Figure 2b, Table S1), indicating homoaggregation. The large standard deviation for the $d_{h,n}$ of these nanoparticles indicates the aggregate sizes were polydisperse. Suspension in the buffer solution had minimal impact on the $d_{h,n}$ of PAA- and EG₆-AuNPs (Figure 2a, Table S1).



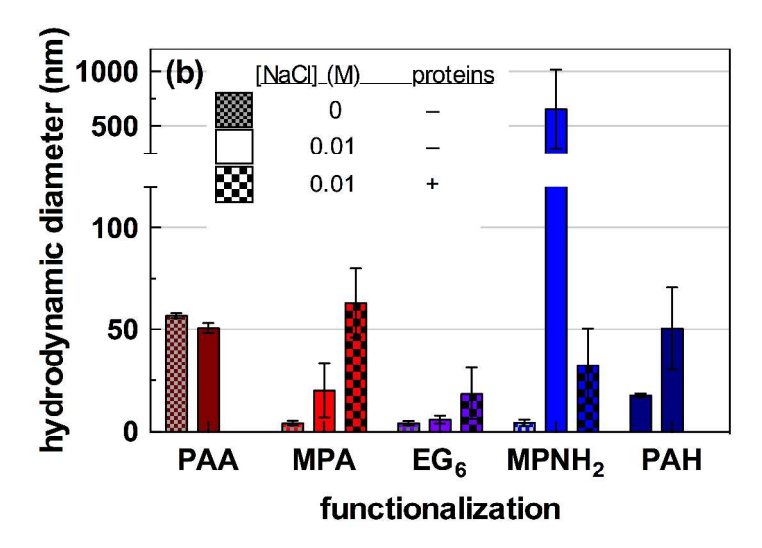


Figure 2. (a) apparent ζ potentials and (b) number mean hydrodynamic diameters ($d_{h,n}$) of functionalized gold nanoparticles (AuNPs) and protein-AuNP complexes. Measurements were made in ultrapure water without proteins or in 0.01 M NaCl buffered to pH 7.4 with 0.01 M Tris in the absence or presence of complexed proteins. Bars represent mean values; error bars correspond to one standard deviation for triplicate experiments. Hydrodynamic diameters are not reported for protein complexes of PAH- and PAA-AuNP because they could not be re-suspended for characterization. Numerical values for ζ potential and $d_{h,n}$ are given in Table S1. Number

mean hydrodynamic diameter distributions are provided in Figure S4. In the legends, + and – indicate the presence or absence of complexed proteins.

Effect of Serum Proteins on the Electrokinetic and Hydrodynamic Properties of AuNPs. Exposure of functionalized AuNPs to serum proteins led to changes in their electrokinetic and hydrodynamic properties. We incubated the functionalized AuNPs in fetal bovine serum (FBS) solution for 60 min to allow protein-AuNP complexes to form and separated these complexes from free and weakly complexed proteins via a series of centrifugation and washing steps comparable to those previously used to operationally define the hard corona on larger nanoparticles.³² The changes in apparent ζ potential, hydrodynamic diameter, and visible absorbance spectra of the particles (Figures 2 and S1) induced by this procedure provide direct evidence of the complexation of AuNPs by serum proteins. Complexation by serum proteins shifted the apparent ζ potential of protein-AuNP complexes, isolated from the FBS solution, closer to that measured for the ensemble of proteins in the FBS solution alone (-16 ± 2 mV), as has been previously reported. For the MPNH₂- and EG₆-AuNPs, complexation by serum proteins reduced their apparent ζ potentials to values similar to that measured for the ensemble of FBS proteins (Figure 2a). For the MPNH₂-AuNPs this represented a reversal of the sign of the ζ potential. The apparent ζ potential of the MPA-AuNPs became less negative upon protein complexation, also approaching that measured for the ensemble of FBS proteins. These data indicate that AuNPs form complexes with proteins in FBS, and that complexation with proteins occurs regardless of the charge of the nanoparticle. Data for PAA- and PAH-AuNPs following complexation with proteins in FBS are not shown due to the inability to adequately resuspend the large protein-nanoparticle complexes that formed.

The effect of protein complexation on AuNP aggregation depended on both the charge and structure of the initial surface coating. The positions of the λ_{max} in the visible absorbance

spectra of the ligand-functionalized AuNPs were minimally perturbed following complexation with serum proteins, regardless of the surface charge of the functionalized AuNPs (Figure S1). The small shift in the $\underline{\lambda_{max}}$ observed for the MPNH2-AuNPs (Figure S1) was likely attributable to changes in the local dielectric environment. 10,37 The hydrodynamic diameters of ligandfunctionalized AuNPs with complexed proteins were larger than those of the corresponding nanoparticles in ultrapure water. Formation of protein-AuNP complexes limited aggregation of MPNH₂-AuNPs relative to that observed in 0.01 M NaCl in the absence of proteins (Figure 2b). This suggests that complex formation with serum proteins stabilized these nanoparticles against the more extensive homoaggregation observed in buffer alone, a behavior previously reported for larger citrate-stabilized and PAH-wrapped AuNPs $(d_{core} \sim 15 \text{ nm})$. The other thiolfunctionalized AuNPs (MPA- and EG₆-AuNPs) show an approximate three-fold increase in their hydrodynamic diameters following complexation with serum proteins relative to the same particles in 0.01 M NaCl (Figure 2b, Table S1). The aggregation of the MPA- and EG₆-AuNP upon complexation with proteins evidenced by the increase in hydrodynamic diameter did not bring the AuNP cores into sufficient proximity to impact their plasmonic properties. 35,36 This could be consistent with the thiol-stabilized AuNPs acquiring a coating of serum proteins that prevents further aggregation. Several structures have been proposed for protein-nanoparticle complexes, including a single nanoparticle surrounded by layers of proteins as well as those composed of several nanoparticles and proteins. 17 The current investigation did not elucidate the structure of the protein-NP complexes. Absorption spectroscopy indicated that the polyelectrolyte-wrapped PAH- and PAA-AuNPs aggregate substantially upon incubation in the FBS solution, as evidenced by a red-shift and substantial broadening of their surface plasmon absorbances (Figure S1). We also noted visible aggregation and sedimentation of these particles

in solution with FBS. In contrast to the MPA- and EG₆-AuNPs, the polyelectrolyte-wrapped AuNPs formed much more extensive aggregates, ultimately leading to the sedimentation of large protein-nanoparticle complexes. We note that the aggregation behavior observed for the AuNPs used in this study appears to be surface chemistry- and media-specific. The 4 nm PAH-AuNPs were previously observed to resist aggregation in *D. magna* and *S. oneidensis* media²⁹ (both of which have appreciable ionic strength), while the MPA-AuNPs were susceptible to aggregation in both. Taking these data together, we ascribe the aggregation of the PAH-AuNPs and PAA-AuNPs in FBS to specific interactions between the layer-by-layer coated AuNPs and serum proteins, rather than a loss of particle stability due to the ionic strength of the medium. Taken together, these findings suggest that the structure of the nanoparticle coating in addition to its charge influences the interaction of nanoparticles with proteins. The conformation, packing, and charge density of the ligands or polymer wrapping on the particle surface may affect how the AuNPs interact with the FBS proteins.

Identification of Proteins in Complexes with AuNPs. We determined the identity and relative abundance of serum proteins forming complexes with each type of functionalized AuNP by LC-MS/MS. We exposed each type of AuNP (Figure 1) to FBS proteins, separated the protein-AuNP complexes by centrifugation and washing, and digested the associated proteins with trypsin prior to LC-MS/MS analysis. At least 100 different serum proteins were associated with AuNPs bearing each type of surface functionalization. We conducted a semi-quantitative analysis to determine the relative abundance of each protein complexed with the AuNPs on a mass:mass (m:m) basis using the exponentially modified protein abundance index (emPAI).³⁸ We identified 24 proteins at an abundance ≥ 0.02 m:m in FBS alone or as part of isolated protein-AuNP complexes (Table 1; these data are organized by mol:mol abundance in the

Supporting Information Table S2). These data indicate that although certain serum proteins complex all of the functionalized AuNPs tested, a unique set of proteins was present in the complexes formed with each type of functionalized AuNP, even those AuNPs with similar ζ potentials (PAA- and MPA-AuNPs, PAH- and MPNH₂-AuNPs; Table 1, Figure 2a).

The most abundant proteins in the FBS were APOA1 (apolipoprotein A-I), A2MG (α -2-macroglobulin), TRFE (serotransferrin), CO3 (complement C3), ALBU (serum albumin), and A1AT (α -1-antiproteinase). Although many of the proteins that form complexes with the AuNPs are abundant in FBS, the most common proteins in FBS were not necessarily the most abundant proteins in complexes with the AuNPs. For example, while serotranferrin ranked among the most abundant proteins in FBS (\sim 0.06 m:m), this protein was not detected in abundance (\geq 0.02 m:m) in complexes with any of the AuNPs investigated. Furthermore, many proteins that were not particularly abundant in FBS (e.g., APOE (apolipoprotein E), TSP1 (thrombospondin), PEDF (pigment epithelium-derived factor), and GELS (gelsolin) \leq 0.02 m:m protein content) were found in relatively high abundance in complexes with several of the AuNPs. Interestingly, a number of proteins in complexes with the AuNPs are involved in binding phospholipids or glycans (based on Gene Ontology annotations; 39,40 viz. APOA1, CO3, ALBU, A1AT, FETUA, APOA2, APOE).

The surface chemistry of the AuNPs clearly influenced the identity of the complexed proteins. No trends were discernable in the size, biological processes and molecular functions (as determined by Gene Ontology annotations; ^{39,40} Figures S5 and S6), and isoelectric point (Figure S7) of the proteins in the protein-AuNP complexes (see the Supporting Information for further discussion). The lack of trend with protein isoelectric point may indicate that any electrostatically driven interactions between nanoparticles and proteins are guided by distinct

regions of charge on the protein surface and cannot be predicted by bulk isoelectric point. Intriguingly, AuNPs of similar size and surface charge, but prepared using distinct ligands or polyelectrolyte wrappings, selected distinct profiles of complexing proteins. For example, a total of 16 proteins formed complexes with the two positively-charged AuNPs (MPNH₂ and PAH) at an abundance ≥ 0.02 m:m. Of these 16 proteins, only six were found to form complexes with both AuNPs. Overlap between the proteins complexing cationic MPNH₂-AuNPs and anionic MPA-AuNPs was more extensive; of the 15 proteins found with m:m ≥ 0.02 complexes of these oppositely charged AuNPs had eight proteins in common. Despite the unique composition of proteins forming complexes with MPA-, EG₆-, and MPNH₂-AuNPs (Table 1), the apparent ζ potential of the protein-AuNP complexes was very similar (Figure 2a).

Selective protein complexation is consistent with previous reports that factors such as nanoparticle size, nanoparticle surface functionalization, and protein-nanoparticle incubation conditions can influence which proteins adsorb to their surfaces from serum solution; nanoparticles do not simply adsorb the most prevalent proteins in serum.^{7,9,41} Of the most abundant proteins complexed with the AuNPs investigated here, several have previously been reported in the coronas of other AuNPs incubated in FBS solutions. For example, the protein corona of CTAB-functionalized gold nanorods (aspect ratio ~4.5) incubated in FBS contained α -2-HS-glycoprotein, serum albumin, α -1-antiproteinase, and hemoglobin fetal subunit- β , ³² and the FBS protein coronas of 15 nm AuNPs with widely varying surface chemistries included α -2-HS-glycoprotein, hemoglobin fetal subunit β , and apolipoprotein A-II.^{14,32,42} We note that a variety of factors can influence the composition of the hard protein corona including nanoparticle concentration, nanoparticle size, ⁴³ incubation time, ⁴⁴ incubation temperature, ⁴⁵ protein source (*e.g.*, FBS vs. human serum or plasma, organ-derived fluids, cytosol), protein concentration, ¹¹

and the ionic strength and composition of the medium. The proteins listed in Table 1 should therefore be regarded as the dominant proteins complexing with the AuNPs tested here under the specific solution conditions used in this study. We expect that differences in protein composition would influence outcomes for the interactions with model cell membranes discussed below.

Interaction of Protein-AuNP Complexes with Supported Lipid Bilayers. Having established that the initial coating of the AuNPs dictates the assemblage of proteins in the hard corona and that ensembles of protein-AuNP complexes differing in protein composition can have the same apparent ζ potential, we investigated the potential cascading effect of initial particle surface coating on interaction with model cell membranes. We constructed supported lipid bilayers on SiO₂-coated QCM-D sensors from small unilamellar vesicles composed of either 1,2dioleoyl-sn-glycero-3-phosphocholine (DOPC) or a 9:1 mass ratio of DOPC and bovine liver αphosphatidylinositol (PI) via the vesicle fusion method. 46 The changes in frequency and energy dissipation observed for both types of bilayer were consistent with those of stable bilayers formed on silica substrates: DOPC, $\Delta f = -24.8 \pm 0.2$, $\Delta D = 0.04 \pm 0.01$; 9:1 DOPC:PI, $\Delta f =$ -24.9 ± 0.2 , $\Delta D = -0.02 \pm 0.01$). ^{22,47} In previous work we have shown that supported lipid bilayers formed in this manner have the expected smoothness and fluidity as determined by atomic force microscopy and fluorescence recovery after photobleaching. 22,47 Lipids bearing a zwitterionic phosphatidylcholine headgroup comprise a large fraction of the lipid components in many eukaryotic cytoplasmic and intracellular membranes. 48 Anionic phosphatidylinositol is a minor component in eukaryotic membranes, its abundance varying among species and types of membranes, but generally comprising <10% of the total phospholipid in mammalian plasma membranes. 48 Phosphatidylinositols are present in both the inner and outer leaflets of the plasma membrane, but are enriched in the inner leaflet.⁴⁹ Their involvement in cell signaling processes

as a membrane binding site for proteins⁴⁹ suggests they may influence the interaction of proteinnanoparticle complexes with cellular membranes. Literature exists on the interaction of some
types of nanoparticles with supported lipid bilayers composed of phospholipids with
phosphotidylcholine headgroups, ^{22,30,31,50–53} but the impact of PI on nanoparticle interaction with
model membranes has not been previously explored. Prior studies employing nanoparticles much
larger than most serum proteins demonstrated that acquisition of a protein corona reduced
interaction with model membranes. ^{15,53} We therefore hypothesized that complexation of the
small nanoparticles studied here by serum proteins would diminish their attachment to model
membranes composed of DOPC alone due to the reduction in nanoparticle surface free energy¹⁵
and increase in steric repulsion between nanoparticles and supported lipid bilayers. ⁵³ Due to the
role of PI in in protein binding we hypothesized that complexation of nanoparticles by proteins
would increase attachment to supported lipid bilayers containing this anionic phospholipid
relative to bilayers composed solely of DOPC.

We employed QCM-D to measure the interaction of AuNPs (with and without complexed proteins) with supported lipid bilayers. This technique measures changes in both the resonance frequency (Δf) and energy dissipation of a coated piezoelectric quartz crystal upon interaction with an analyte. The frequency change is related to the mass of analyte adsorbed to the sensor surface plus any dynamically coupled solvent.⁵⁴ Negative values of Δf indicate an increase in mass attached to the sensor surface. The ζ potential above DOPC bilayers on SiO₂ is negative (-17.5 ± 0.7 mV at pH 7.5 in 0.01 M KCl) as determined by streaming current measurements.⁵⁵ The incorporation of anionic PI into the 9:1 DOPC:PI bilayer is expected to produce a more negative ζ potential than DOPC. The ζ potentials of the small unilamellar vesicles used to form

the bilayers support this expectation. The ζ potential for DOPC vesicles was -1.2 ± 0.8 mV, while that for the 9:1 DOPC:PI vesicles was -29.4 ± 2.8 mV.

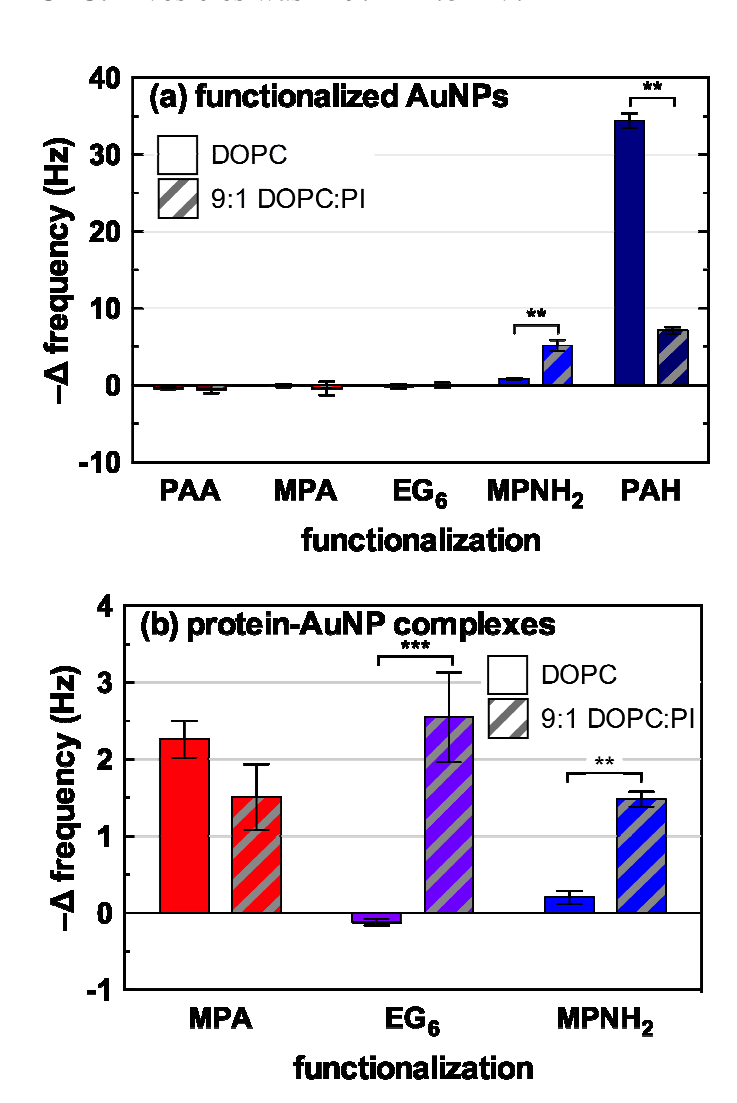


Figure 3. Attachment of (a) functionalized AuNPs or (b) protein-AuNP complexes to bilayers comprised of DOPC and a 9:1 ratio of DOPC and liver α-phosphatidylinositol. Experiments were conducted at pH 7.4 (0.01 M Tris) and 0.01 M NaCl. Reported frequency shifts represent stable values obtained after rinsing. Bars represent mean values, and error bars correspond to one standard deviation for triplicate experiments. Significance of differences between bilayers: **, p < 0.01; ***, p < 0.001).

Interaction of functionalized AuNPs with supported lipid bilayers. We first investigated the attachment of the functionalized AuNPs to supported lipid bilayers composed of DOPC or 9:1 DOPC:PI in 0.01 M NaCl buffered to pH 7.4 with 0.01 M Tris (Figure 3a). No attachment

was observed to either type of bilayer for AuNPs with negative apparent ζ potentials (viz. MPA-, EG₆-, and PAA-AuNPs). Coulombic repulsion explains the lack of observable attachment of the negatively charged PAA-, MPA-, and EG₆-AuNPs (Figure 2a) to bilayers with a negative ζ potential. We note that we have previously demonstrated the attachment of MPA-AuNPs to pure DOPC bilayers at amounts below the limit of QCM-D detection.²²

In contrast, both types of cationic AuNPs (those functionalized with the MPNH₂ ligand and those wrapped in the PAH polymer) attached to both types of bilayers. Attachment of MPNH₂-AuNPs was higher to DOPC:PI bilayers than to DOPC bilayers, while the opposite was true for the PAH-AuNPs. The higher attachment of MPNH2-AuNPs to 9:1 DOPC:PI relative to DOPC bilayers ($-\Delta f = 5.1 \pm 0.8$ Hz and 0.75 ± 0.13 Hz, respectively) is consistent with increased electrostatic attraction due to incorporation of the anionic lipid. The attachment of PAH-AuNPs to 9:1 DOPC:PI bilayers was less than that to pure DOPC bilayer ($-\Delta f = 7.1 \pm 1.0$ Hz and 34.4 ± 1.0 1.0 Hz, respectively). This result is the subject of ongoing work, but may relate to the ability of primary amines in PAH to access the phosphate groups of phosphatidylcholine headgroups; similar decreases in attachment relative to pure DOPC bilayers have been observed upon incorporation of other anionic phospholipids into the bilayers (viz. the corresponding phosphatidylglycerol and phosphatidylserine lipids).⁵⁶ Comparing PAH- and MPNH₂-AuNP attachment to DOPC ($-\Delta f = 34.4 \pm 1.0$ Hz and 0.8 ± 0.1 Hz, respectively), differences are likely influenced by PAH-AuNPs exhibiting a larger positive apparent ζ potential than the MPNH₂-AuNPs ($\pm 4.0 \text{ mV}$ and $\pm 26.9 \pm 1.5 \text{ mV}$, respectively) as well as large differences in aggregate sizes (50.6 \pm 20.3 nm for PAH-AuNPs and 655 \pm 360 nm for MPNH₂-AuNPs). We expect the larger MPNH₂-AuNP aggregates to diffuse more slowly to the bilayer surface, ultimately reducing nanoparticle attachment to the bilayer.

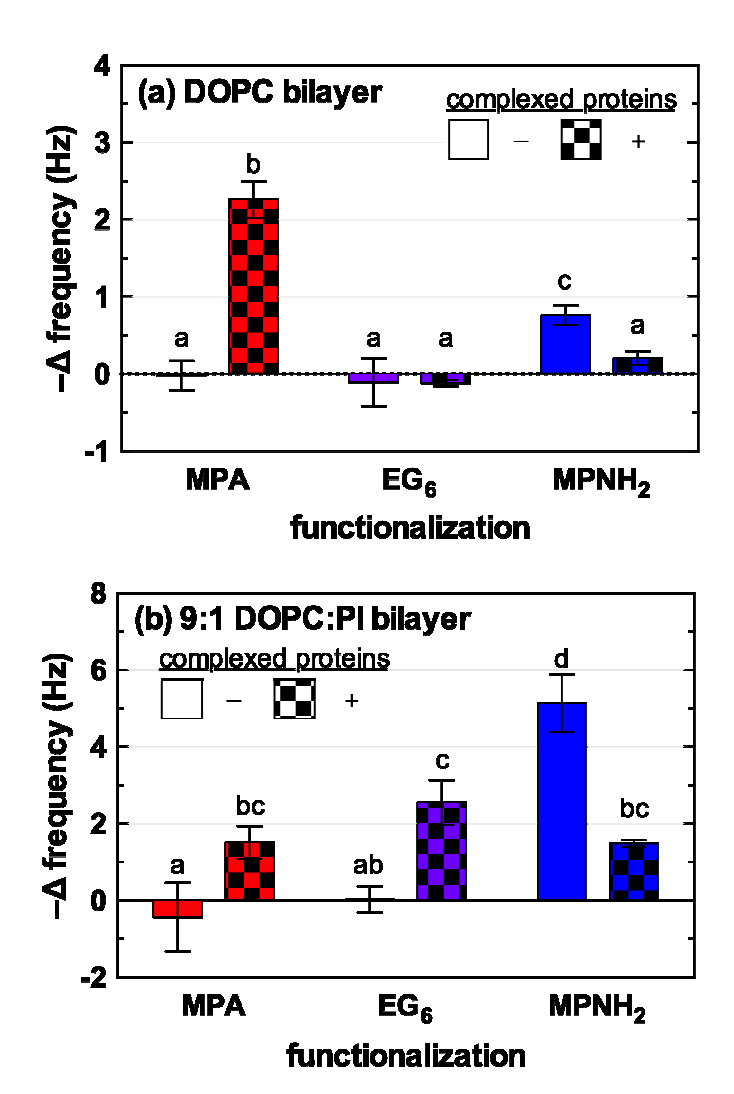


Figure 4. Attachment of functionalized AuNPs without and with complexed proteins to supported lipid bilayers composed of (a) DOPC and (b) a 9:1 mixture of DOPC and liver α-phosphatidylinositol. Experiments were conducted at pH 7.4 (0.01 M Tris) and 0.01 M NaCl. Reported frequency shifts represent stable values obtained after rinsing with nanoparticle-and protein-free solution of otherwise identical composition. Bars represent mean values, and error bars correspond to one standard deviation for triplicate experiments. Letters indicate significant differences in nanoparticle attachment (p < 0.05).

Interaction of protein-AuNP complexes with supported lipid bilayers. We next examined attachment of the protein-AuNP complexes to supported lipid bilayers composed of DOPC or a 9:1 mixture of DOPC and PI to determine the effect of complexed proteins on their interaction with lipid bilayers. For these experiments, we prepared protein-AuNP complexes in the same

manner as we did for characterizing protein-AuNP complexes and identifying proteins complexed with the particles (*vide supra*). As mentioned previously, we were unable to resuspend protein complexes of PAA- and PAH-AuNPs after isolation, and therefore did not conduct QCM-D experiments for these particles with complexed proteins. For nearly all AuNP-bilayer combinations, complexation by serum proteins significantly influenced the extent of attachment to the model membranes (Figure 4, some data from Figure 3 has been replotted to facilitate comparisons for each bilayer type).

For DOPC bilayers, protein complexation increased attachment of MPA-AuNPs (from $-\Delta f \approx 0$ to 2.3 \pm 0.2 Hz; p < 0.05), had no effect on attachment of EG₆-AuNPs, and reduced attachment of the initially cationic MPNH₂-AuNPs (from $-\Delta f = 0.76 \pm 0.13$ to 0.20 ± 0.09 Hz; p < 0.05) (Figure 4a). The reduction in attachment to DOPC observed after formation of protein complexes with MPNH₂-AuNPs can be attributed, at least in part, to electrostatic repulsion as the apparent ζ potential shifted from a positive (+27 ± 2 mV) to a negative (-21 ± 2 mV) value upon complexation with serum proteins (Figure 2a). We note that despite differences in the composition of their protein coronas (Table 1), protein complexes of MPA- and MPNH₂-AuNPs possess statistically indistinguishable apparent ζ potentials (p = 0.32). Despite identical apparent ζ potentials, attachment of protein complexes of MPA-AuNPs to DOPC layers was higher than those of MPNH₂-AuNPs by a factor of approximately ten (Figure 3b). This indicates that the identity, orientation, and/or conformation of the proteins complexing these AuNPs influenced their interaction with the purely zwitterionic bilayer. The increase in attachment of MPA-AuNPs with complexed proteins, as compared to the same nanoparticles without complexed proteins (Figure 4a), was unexpected given our hypothesis that proteins would reduce the nanoparticle surface free energy and increase steric repulsion. This hypothesis was based on results from

phosphatidylcholine lipid bilayers upon adsorption of proteins to nanoparticle surfaces. ^{15,53} We note, however, that complexation of ZnO nanoparticles with bovine serum albumin has been reported to increase interaction with giant unilamellar vesicles composed of DOPC. ⁵⁷ Our results demonstrate that, at least for nanoparticles similar in size to serum proteins, the formation of complexes with proteins does not always diminish adhesion to zwitterionic biomembranes.

We next examined attachment of protein-AuNP complexes to bilayers formed from 9:1 DOPC:PI (Figure 4b). As was the case for DOPC bilayers, complexation by serum proteins promoted attachment of MPA-AuNPs (attachment increased from $-\Delta f = -0.43 \pm 0.89$ Hz to 1.5 \pm 0.4 Hz) and decreased attachment of MPNH₂-AuNP (from $-\Delta f = 5.1 \pm 0.8$ Hz to 1.5 \pm 0.1 Hz). Interestingly, EG₆-AuNPs, which did not interact to a detectable extent with either DOPC (with or without complexed proteins – Figure 4a) or 9:1 DOPC:PI (without complexed proteins – Figure 4b) bilayers, attached to the DOPC:PI bilayer when complexed with serum proteins ($-\Delta f$ = 2.6 ± 0.6 Hz; Figure 4b). All protein-AuNP complexes possessed negative apparent ζ potentials (Figure 2a). The surface potential of the PI-containing bilayers was more negative than that of the DOPC bilayers (vide supra). If the extent of protein-AuNP complex attachment to the bilayers was governed by global electrostatics, attachment would be expected to be lower to bilayers containing anionic PI. In contrast, the attachment of protein complexes of EG₆- and MPNH₂-AuNPs to 9:1 DOPC:PI bilayers exceeded that to DOPC bilayers, and the extent of attachment of these protein-nanoparticle complexes to 9:1 DOPC:PI bilayers did not differ from that of the protein complexes of MPA-AuNPs (Figure 3b). These results support our initial hypothesis. Phosphatidylinositol influenced the interaction of protein-AuNP complexes with

model membranes in a manner suggesting the recognition of and interaction with this anionic phospholipid by specific complexed proteins.

Taking the results from all of the experiments probing the interaction of AuNPs with bilayers in the absence and presence of complexed proteins, we were unable to identify correlations between bulk (protein-)nanoparticle properties (viz. d_h , apparent ζ potential) and several metrics characterizing attachment to DOPC and 9:1 DOPC:PI bilayers (viz. Δf , initial deposition rate, and attachment efficiency⁵⁸). This suggests that the initial coating of the AuNPs drives the identity, orientation, 59-61 and/or conformation (which may expose hidden epitopes), 62-⁶⁵ of complexed proteins which in turn strongly influences nanoparticle interaction with lipid bilayers. Considering only those proteins found in protein-AuNP complexes abundances > 0.02 on a mass:mass basis, five were identified that function in lipid binding (APOA1, ALBU, FETUA, APOA2, and APOE). The presense of lipid-binding proteins in the coronas of nanoparticles suspended in plasma has been previously reported. 66 Over 100 proteins were identified in complexes with each AuNP; we cannot rule out that favorable attachment is governed by lower abundance proteins. We note that biomolecules in addition to proteins are present in FBS (e.g., lipids), ⁶⁷ and that these molecules may also associate with nanoparticles ⁶⁶ and impact membrane binding. The results presented here provide motivation for future studies employing small numbers of proteins to better elucidate the mechanisms of protein-nanoparticle interaction and its cascading effect on nanoparticle-membrane interaction.

CONCLUSIONS

We have demonstrated that for nanoparticles similar in size to serum proteins, the initial nanoparticle surface coating has a cascading effect on interactions with model cell membranes by determining the assemblage of proteins complexing the nanoparticles which in turn influences

subsequent interaction with model biological membranes. We found that the initial nanoparticle surface chemistry leads to stark differences in the collection of proteins complexing the AuNPs. Gold nanoparticles of similar core diameters and presenting the same functional group to solution, yet differing in coating structure (short ligand vs. polymer wrapping), were complexed by distinct sets of serum proteins. A similar result was reported for quaternary amine-containing ligand varying in head-group hydrophobicity.⁶⁸ The composition of hard corona proteins is sensitive to both nanoparticle coating charge, hydrophobicity, and structure. The surface defined by the proteins complexed to nanoparticles dominates the interaction of the protein-nanoparticle complexes with model biological membranes. We have investigated the effect of complexation by proteins on the initial step of nanoparticle-membrane interaction and found that the effect on membrane affinity can be large. We expect that changes to nanoparticle properties due to acquisition of a protein corona also impacts deformation, alteration in membrane structure, and translocation. Future studies will be directed at understanding how complexed proteins impact these downstream interactions. Protein complexes with the same apparent ζ potentials did not interact with model membranes to the same extent. Rather, the initial surface coating dictated the assemblage of proteins complexing the nanoparticles and likely also impacted their orientation^{59,60,69} and conformation.^{62-64,70} This in turn governed interaction with the model membranes. Future studies will employ nanoparticles with more complex surface chemistries, such as zwitterionic ligands, mixed monolayers, and silica coatings. In addition to conferring increased resistance with respect to aggregation, such particles may lead to the identification of more specific protein-nanoparticle interactions. We also found that the composition of the model membrane strongly influenced nanoparticle attachment. Gold nanoparticles functionalized with mercapto-undecanethiol-ethyleneglycol hexamer (EG₆-AuNPs) did not interact with either

membrane studied in the absence of complexed serum proteins; protein complexes of these nanoparticles attached only to lipid bilayers containing the anionic phospholipid phosphatidylinositol. Phosphatidylinositol comprises a relatively small proportion of mammalian cytoplasmic membranes, but is present in higher proportions in the membranes of intracellular organelles. ⁴⁸ Protein complex-mediated interaction with phosphatidylinositol may lead to preferential accumulation in specific organelles. In summary, we found that the charge and structure of the initial coating of small gold nanoparticles organized the assemblages of serum proteins associated with them in a manner that impacted binding to model cell membranes. In addition, the composition of phospholipids in the membrane affected protein-nanoparticle binding suggesting that the influence of other cell surface structures (*e.g.*, proteins, glycans)^{30,31} warrants investigation to more fully understand the nano-bio interface.

MATERIALS AND METHODS

Materials. All materials were used as received, unless otherwise noted. Hydrogen tetrachloroaurate trihydrate (HAuCl₄·3H₂O), sodium borohydride, mercaptopropionic acid, 3amino propanethiol hydrochloride, sodium polyacrylate ($M_r = 15~000~\mathrm{Da}$, 35 wt % in water), polyallylamine HCl ($M_{\rm r}$ = 15 000 Da), and fetal bovine serum were purchased from Sigma Aldrich. Trisodium citrate dihydrate was obtained from Flinn Scientific. The EG₆-undecanethiol procedure.³³ ligand $(HSC_{11}EG_6)$ was synthesized following published Tris(hydroxymethyl)aminomethane (Tris) was purchased from Fisher Scientific. The phospholipids 1,2-dioleoyl-sn-glycero-3-phosphocholine (DOPC) and bovine liver α phosphatidylinositol (PI) were purchased from Avanti Polar Lipids. PI is a mixture of phosphatidylinositol lipids that vary in acyl chain length, the degree of saturation, and the

position of double bonds (the most abundant species in this mixture has two saturated 18-carbon acyl chains).

Ultrapure water (>18 M Ω ·cm) was prepared using a Barnstead Diamond Nanopure or GenPure Pro water filtration system. PALL tangential flow filtration capsules (50 kDa pore size) and 5.0 mL volume Spectra/Por cellulose ester dialysis membranes (50 kDa pore size) were purchased from VWR.

Synthesis and Functionalization of AuNPs. Gold nanoparticles (4 nm core diameter) were prepared by borohydride reduction of HAuCl₄ in the presence of MPNH₂, MPA, hydroxy-EG₆-undecanethiol, or citrate, as previously described. The resulting MPNH₂-, MPA-, and EG₆-AuNP solutions were then purified by diafiltration. Citrate-AuNPs were wrapped with PAH and purified by dialysis, followed by centrifugation and washing. PAA-wrapped AuNPs were prepared from the PAH-AuNPs and purified by dialysis, followed by centrifugation. Further details on AuNP synthesis and purification are provided in the Supporting Information.

Characterization of AuNPs. The core diameters of the purified AuNPs were determined by visible absorbance spectroscopy and TEM analysis. Visible absorption spectra were obtained using a Cary 500 scanning UV-vis spectrophotometer. For TEM studies, purified AuNP solutions were dropcast onto TedPella SiO-Cu mesh TEM grids. TEM images were obtained using a JEOL 2100 Cryo TEM. Size distributions for the dropcast AuNP samples were determined using ImageJ. Hydrodynamic diameters and ζ potentials for the AuNPs were derived from dynamic light scattering (DLS) and electrophoretic light scattering measurements (ELS) obtained using a Malvern Zetasizer Nano ZS.

Formation of Protein-AuNP Complexes Preparation of the protein-AuNP complexes was the same for all experiments, except that a final bath sonication step to aid re-dispersion of

protein-AuNP complexes was included for QCM-D, DLS, and ELS experiments (described below). A sufficient volume of purified AuNP solutions were added to 1.5 mL microcentrifuge tubes to attain a final AuNP number concentration of 12.8 nM. Cold FBS (0 °C, 100 μL) was added to the microcentrifuge tubes, and the tubes were incubated at 37 °C for 20 min. After 20 min, 1.0 mL of Tris buffer solution (0.01 M NaCl, 0.01 M Tris, pH 7.4) was added. The tubes were incubated at 37 °C for 40 min (AuNPs in 10% serum for QCM-D experiments were used immediately following this incubation step). Then, the tubes were centrifuged three times (14 000g, 10 min) with a 4 °C Tris buffer solution wash between each centrifugation step. Finally, the sedimented AuNPs were re-dispersed in Tris buffer to isolate the AuNPs and associated complexed proteins. We note that the reduction in ionic strength may have altered the interaction of the proteins with the AuNPs. For the QCM-D, DLS, and ELS experiments, bath sonication (1 min) was used to aid re-dispersion. We were unable to re-disperse the PAH- and PAA-AuNPs after complexation with serum proteins and centrifugation, and therefore did not investigate these particles in DLS, ELS, and QCM-D experiments.

Identification of Proteins Complexed with AuNPs. Protein-NP complexes were purified by centrifugation and washing, then prepared for LC-MS/MS analysis using a method described previously.³² Briefly, following incubation in FBS, protein-NP complexes were centrifuged (14 500g, 30 min) and the pellet was re-suspended in 4 °C Tris buffer solution. This procedure was repeated twice. Next, 25 μL of Sequencing Grade Trypsin (12.5 ng·mL⁻¹ in 0.025 M ammonium bicarbonate, G-Biosciences St. Louis, MO) was added to the protein-AuNP complexes, which were then digested using a CEM Discover Microwave Digester (Mathews, NC) for 15 min at 55 °C (70 W). Digestion was halted by addition of 200 μL of 50% acetonitrile + 5% formic acid, and the digestate was dried using a Thermo SpeedVac and re-suspended in 13

 μL of 5% acetonitrile + 0.1% formic acid. An aliquot (10 μL) was then injected for mass spectroscopy analysis.

The LC-MS/MS analysis was conducted on a Waters quadrupole time-of-flight mass spectrometer (Q-ToF) connected to a Waters nanoAcquity UPLC. The column used was Waters Atlantis C-18 (0.03 mm particle, 0.075 mm × 150 mm). Flow rate was 250 nL·min⁻¹. Peptides were eluted using a linear gradient of water/acetonitrile containing 0.1% formic acid and 0-60% acetonitrile in 240 min. The mass spectrometer was set for data dependent acquisition, and MS/MS was performed on the four most-abundant peaks at any given time. Data were analyzed using Waters Protein Lynx Global Server 2.2.5, Mascot (Matrix Sciences) and the identity of proteins was determined from the peptide fragments using the NCBI NR database specific for *Bos taurus*.

We semi-quantitatively assessed the abundance of proteins complexing AuNPs bearing each type of functionalization using the Exponentially Modified Protein Abundance Index (emPAI).³⁸ The relative abundance of each protein identified by MS study was calculated as:

protein content (m:m) =
$$\frac{\text{emPAIi}_{i} \times M_{r,i}}{\sum_{i=0}^{n} (\text{emPAIi}_{i} \times M_{r,i})}$$
(1)

where emPAI_i is a relative measure of the abundance of protein i within the sample (provided by the Mascot software), and $M_{r,i}$ is the molecular mass (Da) of protein i. Using this approach, the relative contribution of each protein (normalized for protein mass) to the total complexed protein content on the AuNPs can be determined.

Preparation of Small Unilamellar Vesicles. Small unilamellar phospholipid vesicles (\sim 75 nm) were prepared as described previously.⁴⁷ Briefly, phospholipids dissolved in chloroform were mixed to the appropriate ratio, dried under an ultrapure N_2 stream, and held

under vacuum for at least 1 h. Lipid films were rehydrated with 0.001 M NaCl, pH 7.4 (0.01 M Tris) buffer, subjected to three freeze-thaw cycles (liquid nitrogen followed by bath sonication), and extruded 11 times (Avanti Polar Lipids mini-extruder, 610000) through 50 nm polycarbonate membranes. Vesicle hydrodynamic diameter (d_h , nm) and ζ potential (mV) were determined for all vesicle preparations to ensure uniformity and incorporation of the anionic PI lipids. Stock lipid solutions (2.5 mg·mL⁻¹) were stored at 4 °C and used within one week of preparation.

Nanoparticle Attachment to Supported Lipid Bilayers. We investigated the attachment of the AuNPs and the serum protein-AuNP complexes to supported lipid bilayers using a Biolin Scientific Q-Sense E4 QCM-D instrument. Quartz crystal sensors coated with SiO₂ (OSX 303, Biolin Scientific) were used for all experiments. The flow rate (100 µL·min⁻¹) and temperature (25 °C) were held constant throughout the experiment. The general procedure for each QCM-D experiment was as follows: 0.1 M NaCl, 0.005 M CaCl₂, pH 7.4 (0.01 M Tris) solution was flown until stable values for frequency and dissipation were achieved, lipid vesicles (diluted to 0.125 mg·mL⁻¹ with the CaCl₂-containing buffer) were introduced until a supported lipid bilayer was formed, 47 the bilayer was rinsed subsequently with the solution described above, calcium-free solution, and finally with 0.01 M NaCl, pH 7.4 (0.01 M Tris) solution. We then flowed AuNPs (12.8 nM in 0.01 M NaCl, pH 7.4 (0.01 M Tris) – before or after forming complexes with serum proteins) over the bilayer for 20 min, followed by rinsing with 0.01 M NaCl, pH 7.4 (0.01 M Tris) solution. Experiments were conducted in 0.01 M NaCl because nanoparticle suspensions were not stable at high ionic strength. Data are reported for the 5th harmonic. Data comparisons were made by two-way ANOVA with a Tukey multiple comparisons test at the $p \le 0.05$ level of significance.

ASSOCIATED CONTENT

Supporting Information Available

The Supporting Information, and is available free of charge *via* the Internet on the ACS Publications website at http://pubs.acs.org.

Supplementary methods and data including AuNP size distribution histograms, TEM images, DLS/ ζ potential data, and more comprehensive lists of the protein components of complexes with AuNPs.

AUTHOR INFORMATION

Corresponding Authors

*E-mail: joelpedersen@wisc.edu

*E-mail: murphycj@illinois.edu

Present Addresses for SEL: Colorado Mesa University, Department of Chemistry, 1100 North Ave, Grand Junction, CO, 81501

Author Contributions. SEL and AMV synthesized and characterized the AuNPs. BAP synthesized the HSC₁₁EG₆ ligand. SEL, JEP, ESM, and HBA prepared and characterized protein-AuNP complexes. ESM conducted the QCM-D experiments. CJM, JAP and RJH oversaw the design and execution of the experiments and the interpretation of results. ESM, SEL, JEP, RJH, CJM, and JAP wrote the manuscript.

Notes

The authors declare no competing financial interests.

ACKNOWLEDGMENTS

This work was supported by the National Science, CHE-1503408 for the Center for Sustainable Nanotechnology. We thank Peter Yau and the University of Illinois Urbana-Champaign Roy A. Carver Biotechnology Center for assistance with the LC-MS/MS analysis and data interpretation.

ABBREVIATIONS. AuNP, gold nanoparticle; DLS, dynamic light scattering; LC-MS/MS, liquid chromatography-tandem mass spectrometry; MPA, mercaptopropanoic acid; MPNH₂, mercaptopropylamine; PAA, polyacrylic acid; PAH, poly(allylamine HCl); PC, phosphatidylcholine; PI, phosphatidylinositol; QCM-D, quartz crystal microbalance with dissipation monitoring; supported lipid bilayer, supported lipid bilayer; TEM, transmission electron microscopy.

REFERENCES

- (1) Walkey, C. D.; Chan, W. C. W. Understanding and Controlling the Interaction of Nanomaterials with Proteins in a Physiological Environment. *Chem. Soc. Rev.* **2012**, *41*, 2780–2799.
- (2) Verma, A.; Stellacci, F. Effect of Surface Properties on Nanoparticle-Cell Interactions. *Small* **2010**, *6*, 12–21.
- (3) Monopoli, M. P.; Walczyk, D.; Campbell, A.; Elia, G.; Lynch, I.; Bombelli, F. B.; Dawson, K. A. Physical-Chemical Aspects of Protein Corona: Relevance to in Vitro and in Vivo Biological Impacts of Nanoparticles. *J. Am. Chem. Soc.* **2011**, *133*, 2525–2534.
- (4) Petros, R. A.; DeSimone, J. M. Strategies in the Design of Nanoparticles for Therapeutic Applications. *Nat. Rev. Drug Discov.* **2010**, *9*, 615–627.
- (5) Salvati, A.; Pitek, A. S.; Monopoli, M. P.; Prapainop, K.; Bombelli, F. B.; Hristov, D. R.; Kelly, P. M.; Åberg, C.; Mahon, E.; Dawson, K. A. Transferrin-Functionalized Nanoparticles Lose Their Targeting Capabilities When a Biomolecule Corona Adsorbs on the Surface. *Nat. Nanotechnol.* **2013**, *8*, 137–143.
- (6) Kumar, A.; Bicer, E. M.; Morgan, A. B.; Pfeffer, P. E.; Monopoli, M. P.; Dawson, K. A.; Eriksson, J.; Edwards, K.; Lynham, S.; Arno, M.; Behndig, A. F.; Blomberg, A.; Somers, G.; Hassal, D.; Dailey, L. A.; Forbes, B.; Mudway, I. S. Enrichment of Immunoregulatory

- Proteins in the Biomolecular Corona of Nanoparticles within Human Respiratory Tract Lining Fluid. *Nanomed-Nanotechnol* **2016**, *12*, 1033–1043.
- (7) Casals, E.; Pfaller, T.; Duschl, A.; Oostingh, G. J.; Puntes, V. Time Evolution of the Nanoparticle Protein Corona. *ACS Nano* **2010**, *4*, 3623–3632.
- (8) Yang, J. A.; Murphy, C. J. Evidence for Patchy Lipid Layers on Gold Nanoparticle Surfaces. *Langmuir* **2012**, *28*, 5404–5416.
- (9) Cedervall, T.; Lynch, I.; Lindman, S.; Berggård, T.; Thulin, E.; Nilsson, H.; Dawson, K. A.; Linse, S. Understanding the Nanoparticle-Protein Corona Using Methods to Quantify Exchange Rates and Affinities of Proteins for Nanoparticles. *Proc. Natl. Acad. Sci. U. S. A.* 2007, 104, 2050–2055.
- (10) Yang, J. A.; Lohse, S. E.; Murphy, C. J. Tuning Cellular Response to Nanoparticles via Surface Chemistry and Aggregation. *Small* **2014**, *10*, 1642–1651.
- (11) Monopoli, M. P.; Aberg, C.; Salvati, A.; Dawson, K. A. Biomolecular Coronas Provide the Biological Identity of Nanosized Materials. *Nat. Nanotechnol.* **2012**, *7*, 779–786.
- (12) Walczyk, D.; Bombelli, F. B.; Monopoli, M. P.; Lynch, I.; Dawson, K. A. What the Cell "Sees" in Bionanoscience. *J. Am. Chem. Soc.* **2010**, *132*, 5761–5768.
- (13) Lundqvist, M.; Stigler, J.; Elia, G.; Lynch, I.; Cedervall, T.; Dawson, K. A. Nanoparticle Size and Surface Properties Determine the Protein Corona with Possible Implications for Biological Impacts. *Proc. Natl. Acad. Sci. U. S. A.* **2008**, *105*, 14265–14270.
- (14) Walkey, C. D.; Olsen, J. B.; Song, F.; Liu, R.; Guo, H.; Olsen, D. W. H.; Cohen, Y.; Emili, A.; Chan, W. C. W. Protein Corona Fingerprinting Predicts the Cellular Interaction of Gold and Silver Nanoparticles. *ACS Nano* **2014**, *8*, 2439–2455.
- (15) Lesniak, A.; Salvati, A.; Santos-Martinez, M. J.; Radomski, M. W.; Dawson, K. A.; Åberg, C. Nanoparticle Adhesion to the Cell Membrane and Its Effect on Nanoparticle Uptake Efficiency. *J. Am. Chem. Soc.* **2013**, *135*, 1438–1444.
- (16) Mahmoudi, M.; Shokrgozar, M. A.; Behzadi, S. Slight Temperature Changes Affect Protein Affinity and Cellular Uptake/toxicity of Nanoparticles. *Nanoscale* 2013, 5, 3240–3244.
- (17) Liu, W.; Rose, J.; Plantevin, S.; Auffan, M.; Bottero, J.-Y.; Vidaud, C. Protein Corona Formation for Nanomaterials and Proteins of a Similar Size: Hard or Soft Corona? *Nanoscale* **2013**, *5*, 1658–1668.
- (18) Mahmoudi, M.; Lynch, I.; Ejtehadi, M. R.; Monopoli, M. P.; Bombelli, F. B.; Laurent, S. Protein-Nanoparticle Interactions: Opportunities and Challenges. *Chem. Rev.* **2011**, *111*, 5610–5637.

- (19) Jiang, X.; Weise, S.; Hafner, M.; Röcker, C.; Zhang, F.; Parak, W. J.; Nienhaus, U.; Jiang, X.; Weise, S.; Hafner, M.; Ro, C. Quantitative Analysis of the Protein Corona on FePt Nanoparticles Formed by Transferrin Binding Quantitative Analysis of the Protein Corona on FePt Nanoparticles Formed by Transferrin Binding. *Interface* 2010, 7, S5–S13.
- (20) Verma, A.; Uzun, O.; Hu, Y.; Hu, Y.; Han, H.-S.; Watson, N.; Chen, S.; Irvine, D. J.; Stellacci, F. Surface-Structure-Regulated Cell-Membrane Penetration by Monolayer-Protected Nanoparticles. *Nat. Mater.* **2008**, *7*, 588–595.
- (21) Wang, T.; Bai, J.; Jiang, X.; Nienhaus, G. U. Cellular Uptake of Nanoparticles by Membrane Penetration: A Study Combining Confocal Microscopy with FTIR Spectroelectrochemistry. *ACS Nano* **2012**, *6*, 1251–1259.
- (22) Troiano, J. M.; Olenick, L. L.; Kuech, T. R.; Melby, E. S.; Hu, D.; Lohse, S. E.; Mensch, A. C.; Dogangun, M.; Vartanian, A. M.; Torelli, M. D.; Ehimiaghe, E.; Walter, S. R.; Fu, L.; Anderton, C. R.; Zhu, Z.; Wang, H.; Orr, G.; Murphy, C. J.; Hamers, R. J.; Pedersen, J. A.; et al. Direct Probes of 4 Nm Diameter Gold Nanoparticles Interacting with Supported Lipid Bilayers. J. Phys. Chem. C 2015, 119, 534–546.
- (23) Leroueil, P. R.; Berry, S. A.; Duthie, K.; Han, G.; Rotello, V. M.; McNerny, D. Q.; Baker, J. R.; Orr, B. G.; Banaszak Holl, M. M. Wide Varieties of Cationic Nanoparticles Induce Defects in Supported Lipid Bilayers. *Nano Lett.* **2008**, *8*, 420–424.
- (24) Harper, S. L.; Carriere, J. L.; Miller, J. M.; Hutchison, J. E.; Maddux, B. L. S.; Tanguay, R. L. Systematic Evaluation of Nanomaterial Toxicity: Utility of Standardized Materials and Rapid Assays. *ACS Nano* **2011**, *5*, 4688–4697.
- (25) Sugio, S.; Kashima, A.; Mochizuki, S.; Noda, M.; Kobayashi, K. Crystal Structure of Human Serum Albumin at 2.5 Å Resolution. *Protein Eng.* **1999**, *12*, 439–446.
- (26) Dreaden, E. C.; Alkilany, A. M.; Huang, X.; Murphy, C. J.; El-Sayed, M. A. The Golden Age: Gold Nanoparticles for Biomedicine. *Chem. Soc. Rev.* **2012**, *41*, 2740.
- (27) West, J. L.; Halas, N. J. Engineered Nanomaterials for Biophotonics Applications: Improving Sensing, Imaging, and Therapeutics. *Annu. Rev. Biomed. Eng.* **2003**, *5*, 285–292.
- (28) Sardar, R.; Funston, A. M.; Mulvaney, P.; Murray, R. W. Gold Nanoparticles: Past, Present, and Future. *Langmuir* **2009**, *25*, 13840–13851.
- (29) Qiu, T. A.; Bozich, J. S.; Lohse, S. E.; Vartanian, A. M.; Jacob, L. M.; Meyer, B. M.; Gunsolus, I. L.; Niemuth, N. J.; Murphy, C. J.; Haynes, C. L.; Klaper, R. D. Gene Expression as an Indicator of the Molecular Response and Toxicity in the Bacterium Shewanella Oneidensis and the Water Flea Daphnia Magna Exposed to Functionalized Gold Nanoparticles. *Environ. Sci. Nano* **2015**, *2*, 615–629.

- (30) Jacobson, K. H.; Gunsolus, I. L.; Kuech, T. R.; Troiano, J. M.; Melby, E. S.; Lohse, S. E.; Hu, D.; Chrisler, W. B.; Murphy, C. J.; Orr, G.; Geiger, F. M.; Haynes, C. L.; Pedersen, J. A. Lipopolysaccharide Density and Structure Govern the Extent and Distance of Nanoparticle Interaction with Actual and Model Bacterial Outer Membranes. *Environ. Sci. Technol.* 2015, 49, 10642–10650.
- (31) Melby, E. S.; Mensch, A. C.; Lohse, S. E.; Hu, D.; Orr, G.; Murphy, C. J.; Hamers, R. J.; Pedersen, J. A. Formation of Supported Lipid Bilayers Containing Phase-Segregated Domains and Their Interaction with Gold Nanoparticles. *Environ. Sci. Nano* **2016**, *3*, 45–55.
- (32) Mahmoudi, M.; Lohse, S. E.; Murphy, C. J.; Fathizadeh, A.; Montazeri, A.; Suslick, K. S. Variation of Protein Corona Composition of Gold Nanoparticles Following Plasmonic Heating. *Nano Lett.* **2014**, *14*, 6–12.
- (33) Pale-Grosdemange, C.; Simon, E. S.; Prime, K. L.; Whitesides, G. M. Formation of Self-Assembled Monolayers by Chemisorption of Derivatives of Oligo(ethylene Glycol) of Structure HS(CH2)11(OCH2CH2)mOH on Gold. *J. Am. Chem. Soc.* **1991**, *113*, 12–20.
- (34) Haiss, W.; Thanh, N. T. K.; Aveyard, J.; Fernig, D. G. Determination of Size and Concentration of Gold Nanoparticles from UV Vis Spectra. *Anal. Chem.* **2007**, *79*, 4215–4221.
- (35) Westcott, S. L.; Oldenburg, S. J.; Lee, T. R.; Halas, N. J. Construction of Simple Gold Nanoparticle Aggregates with Controlled Plasmon–plasmon Interactions. *Chem. Phys. Lett.* **1999**, *300*, 651–655.
- (36) Sönnichsen, C.; Reinhard, B. M.; Liphardt, J.; Alivisatos, A. P. A Molecular Ruler Based on Plasmon Coupling of Single Gold and Silver Nanoparticles. *Nat. Biotechnol.* **2005**, *23*, 741–745.
- (37) Gole, A.; Murphy, C. J. Polyelectrolyte-Coated Gold Nanorods: Synthesis, Characterization and Immobilization. *Chem. Mater.* **2005**, *17*, 1325–1330.
- (38) Ishihama, Y.; Oda, Y.; Tabata, T.; Sato, T.; Nagasu, T.; Rappsilber, J.; Mann, M. Exponentially Modified Protein Abundance Index (emPAI) for Estimation of Absolute Protein Amount in Proteomics by the Number of Sequenced Peptides per Protein. *Mol. Cell. Proteomics* **2005**, *4*, 1265–1272.
- (39) Ashburner, M.; Ball, C.; Blake, J.; Botstein, D.; Butler, H.; Cherry, J.; Davis, A.; Dolinski, K.; Dwight, S.; Eppig, J.; Harris, M. A.; Hill, D. P.; Issel-Tarver, L.; Kasarskis, A.; Lewis, S.; Matese, J. C.; Richardson, J. E.; Ringwald, M.; Rubin, G. M.; Sherlock, G. Gene Ontology: Tool for the Unification of Biology. *Nat. Genet.* **2000**, *25*, 25–29.
- (40) Consortium, T. G. O. Gene Ontology Consortium: Going Forward. Nucleic Acids Res.

, *43*, 1049–1056.

- (41) Eigenheer, R.; Castellanos, E. R.; Nakamoto, M. Y.; Gerner, K. T.; Lampe, A. M.; Wheeler, K. E. Silver Nanoparticle Protein Corona Composition Compared across Engineered Particle Properties and Environmentally Relevant Reaction Conditions. *Environ. Sci. Nano* 2014, 1, 238.
- (42) Sacchetti, C.; Motamedchaboki, K.; Magrini, A.; Palmieri, G.; Mattei, M.; Bernardini, S.; Rosato, N.; Bottini, N.; Bottini, M. Surface Polyethylene Glycol Conformation Influences the Protein Corona of Polyethylene Glycol-Modified Single-Walled Carbon Nanotubes: Potential Implications on Biological Performance. *ACS Nano* **2013**, *7*, 1974–1989.
- (43) Tenzer, S.; Docter, D.; Rosfa, S.; Wlodarski, A.; Kuharev, J.; Rekik, A.; Knauer, S. K.; Bantz, C.; Nawroth, T.; Bier, C.; Sirirattanapan, J.; Mann, W.; Treuel, L.; Zellner, R.; Maskos, M.; Schild, H.; Stauber, R. H. Nanoparticle Size Is a Critical Physicochemical Determinant of the Human Blood Plasma Corona: A Comprehensive Quantitative Proteomic Analysis. *ACS Nano* **2011**, *5*, 7155–7167.
- (44) Lundqvist, M.; Stigler, J.; Cedervall, T.; Berggård, T.; Flanagan, M. B.; Lynch, I.; Elia, G.; Dawson, K. The Evolution of the Protein Corona around Nanoparticles: A Test Study. *ACS Nano* **2011**, *5*, 7503–7509.
- (45) Mahmoudi, M.; Abdelmonem, A. M.; Behzadi, S.; Clement, J. H.; Dutz, S.; Ejtehadi, M. R.; Hartmann, R.; Kantner, K.; Linne, U.; Maffre, P.; Metzler, S.; Moghadam, M. K.; Pfeiffer, C.; Rezaei, M.; Ruiz-Lozano, P.; Serpooshan, V.; Shokrgozar, M. A.; Nienhaus, G. U.; Parak, W. J. Temperature: The "Ignored" Factor at the NanoBio Interface. ACS Nano 2013, 7, 6555–6562.
- (46) Castellana, E. T.; Cremer, P. S. Solid Supported Lipid Bilayers: From Biophysical Studies to Sensor Design. *Surf. Sci. Rep.* **2006**, *61*, 429–444.
- (47) Cho, N.-J.; Frank, C. W.; Kasemo, B.; Höök, F. Quartz Crystal Microbalance with Dissipation Monitoring of Supported Lipid Bilayers on Various Substrates. *Nat. Protoc.* **2010**, *5*, 1096–1106.
- (48) van Meer, G.; Voelker, D. R.; Feigenson, G. W. Membrane Lipids: Where They Are and How They Behave. *Nat. Rev. Mol. Cell Biol.* **2008**, *9*, 112–124.
- (49) Luckey, M. *Membrane Structural Biology with Biochemical and Biophysical Foundations*; 2nd ed.; Cambridge University Press: Cambridge, UK, 2014.
- (50) Yi, P.; Chen, K. L. Interaction of Multiwalled Carbon Nanotubes with Supported Lipid Bilayers and Vesicles as Model Biological Membranes. *Environ. Sci. Technol.* **2013**, *47*, 5711–5719.

- (51) Dogangun, M.; Hang, M. N.; Troiano, J. M.; Mcgeachy, A. C.; Melby, E. S.; Pedersen, J. A.; Hamers, R. J.; Geiger, F. M. Alteration of Membrane Compositional Asymmetry by LiCoO2 Nanosheets. ACS Nano 2015, 9, 8755–8765.
- (52) Mecke, A.; Lee, D. K.; Ramamoorthy, A.; Orr, B. G.; Banaszak Holl, M. M. Synthetic and Natural Polycationic Polymer Nanoparticles Interact Selectively with Fluid-Phase Domains of DMPC Lipid Bilayers. *Langmuir* **2005**, *21*, 8588–8590.
- (53) Wang, Q.; Lim, M.; Liu, X.; Wang, Z.; Chen, K. L. Influence of Solution Chemistry and Soft Protein Coronas on the Interactions of Silver Nanoparticles with Model Biological Membranes. *Environ. Sci. Technol.* **2016**, *50*, 2301–2309.
- (54) Rodahl, M.; Höök, F.; Krozer, A.; Brzezinski, P.; Kasemo, B. Quartz Crystal Microbalance Setup for Frequency and Q-Factor Measurements in Gaseous and Liquid Environments. *Rev. Sci. Instrum.* **1995**, *66*, 3924–3930.
- (55) Zimmermann, R.; Küttner, D.; Renner, L.; Kaufmann, M.; Zitzmann, J.; Müller, M.; Werner, C. Charging and Structure of Zwitterionic Supported Bilayer Lipid Membranes Studied by Streaming Current Measurements, Fluorescence Microscopy, and Attenuated Total Reflection Fourier Transform Infrared Spectroscopy. *Biointerphases* **2009**, *4*, 1–6.
- (56) Kuech, T. R. Biological Interactions and Environmental Transformations of Nanomaterials, University of Wisconsin, Madison, 2015.
- (57) Churchman, A. H.; Wallace, R.; Milne, S. J.; Brown, A. P.; Brydson, R.; Beales, P. A. Serum Albumin Enhances the Membrane Activity of ZnO Nanoparticles. *Chem. Commun.* **2013**, *49*, 4172–4174.
- (58) Quevedo, I. R.; Tufenkji, N. Influence of Solution Chemistry on the Deposition and Detachment Kinetics of a CdTe Quantum Dot Examined Using a Quartz Crystal Microbalance Influence of Solution Chemistry on the Deposition and Detachment Kinetics of a CdTe Quantum Dot Examined Using a Q. *Environ. Sci. Technol.* **2009**, *43*, 3176–3182.
- (59) Yang, J. A.; Johnson, B. J.; Wu, S.; Woods, W. S.; George, J. M.; Murphy, C. J. A Study of Wild Type Alpha Synuclein Binding and Orientation on Gold Nanoparticles. *Langmuir* **2013**, *29*, 4603–4615.
- (60) Shrivastava, S.; McCallum, S. A.; Nuffer, J. H.; Qian, X.; Siegel, R. W.; Dordick, J. S. Identifying Specific Protein Residues That Guide Surface Interactions and Orientation on Silica Nanoparticles. *Langmuir* **2013**, *29*, 10841–10849.
- (61) Calzolai, L.; Franchini, F.; Gilliland, D.; Rossi, F. Protein--Nanoparticle Interaction: Identification of the Ubiquitin--Gold Nanoparticle Interaction Site. *Nano Lett.* **2010**, *10*, 3101–3105.

- (62) Shang, W.; Nuffer, J. H.; Muñiz-Papandrea, V. A.; Colón, W.; Siegel, R. W.; Dordick, J. S. Cytochrome c on Silica Nanoparticles: Influence of Nanoparticle Size on Protein Structure, Stability, and Activity. *Small* 2009, 5, 470–476.
- (63) Aubin-Tam, M.; Hamad-Schifferli, K. Gold Nanoparticle-Cytochrome c Complexes: The Effect of Nanoparticle Ligand Charge on Protein Structure. *Langmuir* 2005, 21, 12080– 12084.
- (64) Vertegel, A. A.; Siegel, R. W.; Dordick, J. S. Silica Nanoparticle Size Influences the Structure and Enzymatic Activity of Adsorbed Lysozyme. *Langmuir* **2004**, *20*, 6800–6807.
- (65) Chen, P.; Seabrook, S.; Epa, V.; Kurabayashi, K.; Barnard, A.; Winkler, D.; Kirby, J.; Ke, P. Contrasting Effects of Nanoparticle Binding on Protein Denaturation. *J. Phys. Chem. C* 2014, 118, 22069–22078.
- (66) Hellstrand, E.; Lynch, I.; Andersson, A.; Drakenberg, T.; Dahlbäck, B.; Dawson, K. A.; Linse, S.; Cedervall, T. Complete High-Density Lipoproteins in Nanoparticle Corona. FEBS J. 2009, 276, 3372–3381.
- (67) Lagarde, M.; Sicard, B.; Guichardant, M.; Felisi, O.; Dechavanne, M. Fatty Acid Composition in Native and Cultured Human Endothelial Cells. *In Vitro* **1984**, *20*, 33–37.
- (68) Saha, K.; Rahimi, M.; Yazdani, M.; Kim, S.; Moyano, D.; Hou, S.; Das, R.; Mout, R.; Rezaee, F.; Mahmoudi, M.; Rotello, V. M. Regulation of Macrophage Recognition through the Interplay of Nanoparticle Surface Functionality and Protein Corona. *ACS Nano* **2016**, *10*, 4421–4430.
- (69) Lin, W.; Insley, T.; Tuttle, M.; Zhu, L.; Berthold, D.; Kral, P.; Rienstra, C.; Murphy, C. Control of Protein Orientation on Gold Nanoparticles. *J. Phys. Chem. C* **2015**, *119*, 21035–21043.
- (70) Fleischer, C.; Payne, C. Secondary Structure of Corona Proteins Determines the Cell Surface Receptors Used by Nanoparticles. *J. Phys. Chem. B* **2014**, *118*, 14017–14026.
- (71) Sweeney, S. F.; Woehrle, G. H.; Hutchison, J. E. Rapid Purification and Size Separation of Gold Nanoparticles via Diafiltration. *J. Am. Chem. Soc.* **2006**, *128*, 3190–3197.
- (72) Brust, M.; Walker, M.; Bethell, D.; Schiffrin, D. J.; Whyman, R. Synthesis of Thiol-Derivatised Gold Nanoparticles in a Two-Phase Liquid-Liquid System. *J. Chem. Soc. Chem. Commun.* **1994**, 801–802.
- (73) Li, Y.; Zaluzhna, O.; Zangmeister, C. D.; Allison, T. C.; Tong, Y. J. Different Mechanisms Govern the Two-Phase Brust Schiffrin Dialkylditelluride Syntheses of Ag and Au Nanoparticles. *J. Am. Chem. Soc.* **2012**, *134*, 1990–1992.

(74) Woehrle, G. H.; Hutchison, J. E.; Özkar, S.; Finke, R. G. Analysis of Nanoparticle Transmission Electron Microscopy Data Using a Public-Domain Image-Processing Program, Image. *Turkish J. Chem.* **2006**, *30*, 1–13.

Table 1. Most Abundant Proteins in Fetal Bovine Serum (FBS) and in Complexes with AuNPs.

				Protein Content (m:m)					
				AuNP functionalization					
Swiss-Prot entry name (protein) ^a	$M_{\rm r}$ (Da)	p <i>I</i>	FBS	РАН	$MPNH_2$	HS-C ₁₁ - EG ₆	MPA	PAA	
APOA1 (apolipoprotein A-I)	28 432	5.5 7	0.11 ± 0.04	0.03 ± 0.03	0.05 ± 0.00	0.04 ± 0.03		0.04 ± 0.02	
A2MG (α-2-macroglobulin)	165 052	5.6 8	0.08 ± 0.01		0.04 ± 0.01	0.04 ± 0.00		0.04 ± 0.03	
TRFE (serotransferrin)	75 830	6.5 0	0.06 ± 0.01						
CO3 (complement C3)	185 047	6.3 7	0.06 ± 0.00	0.02 ± 0.02	0.04 ± 0.00		0.05 ± 0.01	0.03 ± 0.01	
ALBU (serum albumin)	66 433	5.6 0	0.06 ± 0.01	0.11 ± 0.08	0.03 ± 0.00	0.11 ± 0.03	0.03 ± 0.01	0.09 ± 0.00	
A1AT (α-1-antiproteinase)	43 694	5.9 8	0.05 ± 0.02	0.03 ± 0.03	0.03 ± 0.00	0.11 ± 0.02		0.05 ± 0.03	
SPA31 (serpin A3-1)	43 641	5.4 1	0.04 ± 0.01						
HBBF (hemoglobin fetal subunit β)	15 859	6.5 1	0.03 ± 0.01	0.04 ± 0.04	0.05 ± 0.01	0.05 ± 0.02	0.04 ± 0.00	0.06 ± 0.03	
ITIH4 (inter-α-trypsin inhibitor heavy chain)	98 686	5.9 9	0.02 ± 0.01		0.02 ± 0.00				
A5D7R6 (n/a)	104 118	7.7 5	0.02 ± 0.01	0.03 ± 0.01		0.02 ± 0.00			
TTHY (transthyretin)	13 557	5.9 1	0.02 ± 0.01	• -					
A1AG (α-1-acid glycoprotein)	21 253	5.6	0.02 ± 0.01						
FETUA (α-2-HS-glycoprotein)	36 353	5.1	0.02 ± 0.00	$\begin{array}{c} 0.04 \pm \\ 0.01 \end{array}$		0.02 ± 0.01		0.03 ± 0.01	

FETUB (fetuin B)	40 846	5.5 9	0.02 ± 0.00			0.02 ± 0.00		
APOA2 (apololipoprotein A-II)	9 319	8.2	0.02 ± 0.01	0.04 ± 0.04		0.00		
FETA (α-fetoprotein)	66 412	5.9 2	0.02 ± 0.01			0.02 ± 0.01		0.02 ± 0.02
E1BH06 (n/a)	190 527	7.1 1	0.01 ± 0.01		0.04 ± 0.01	0.01	0.07 ± 0.00	0.02 0.05 ± 0.02
GELS (gelsolin)	80 731	5.5 4	0.01 ± 0.00		$\begin{array}{c} 0.02 \pm \\ 0.00 \end{array}$		0.06 ± 0.01	0.04 ± 0.01
PEDF (pigment epithelium- derived factor)	44 056	6.3 1	0.01 ± 0.00		0.02 ± 0.00	$\begin{array}{c} \textbf{0.05} \pm \\ \textbf{0.01} \end{array}$	0.02 ± 0.00	0.02 ± 0.01
APOE (apolipoprotein E)	34 126	5.4 4	0.004 ± 0.002	0.03 ± 0.02	0.04 ± 0.01	0.07 ± 0.02	0.03 ± 0.00	0.05 ± 0.02
TSP1 (thrombospondin-1)	127 741	4.7	0.003 ± 0.001		0.04 ± 0.01	0.06 ± 0.01	0.09 ± 0.02	0.04 ± 0.03
F1MDH3 (n/a)	270 815	5.8 1	0.00 ± 0.00		0.02 ± 0.00			
CFAH (complement factor H)	138 259	6.3	0.001 ± 0.001		0.00		0.03 ± 0.01	0.02 ± 0.01
PLMN (plasminogen)	88 393	7.3 9	0.001 ± 0.000				0.03 ± 0.01	0.01

^a Proteins listed in order of abundance in FBS. Proteins in FBS or complexed to AuNPs with protein content ≥ 0.02 on a mass:mass basis. Those with protein content values ≥ 0.05 in bold. See experimental section for details on protein quantification.

1 TOC Graphic

